Fault-Tolerant Thresholds for the Surface Code in Excess of 5% under Biased Noise

David K. Tuckett⊙, Stephen D. Bartlett⊙, Steven T. Flammia⊙, and Benjamin J. Brown⊙

Centre for Engineered Quantum Systems, School of Physics, University of Sydney, Sydney, New South Wales 2006, Australia

Noise in quantum computing is countered with quantum error correction. Achieving optimal performance will require tailoring codes and decoding algorithms to account for features of realistic noise, such as the common situation where the noise is biased towards dephasing. Here we introduce an efficient high-threshold decoder for a noise-tailored surface code based on minimum-weight perfect matching. The decoder exploits the symmetries of its syndrome under the action of biased noise and generalizes to the fault-tolerant regime where measurements are unreliable. Using this decoder, we obtain fault-tolerant thresholds in excess of 6% for a phenomenological noise model in the limit where dephasing dominates. These gains persist even for modest noise biases: we find a threshold of ∼5% in an experimentally relevant regime where dephasing errors occur at a rate 100 times greater than bit-flip errors.

The surface code [1,2] is among the most promising quantum error-correcting codes to realize the first generation of scalable quantum computers [3–5]. This is due to its two-dimensional layout and low-weight stabilizers that help give it its high threshold [1,6,7], and its universal set of fault-tolerant logical gates [1,8–11]. Ongoing experimental work [12–15] is steadily improving the surface code error rates. Concurrent work on improved decoding algorithms [6,7,16–19] is leading to higher thresholds and lower logical failure rates, reducing the exquisite control demanded of experimentalists to realize such a system.

Identifying the best decoder for the surface code depends critically on the noise model. Minimum-weight perfect matching (MWPM) [20,21] is near optimal in the case of the standard surface code with a bit-flip noise model [1] and for a phenomenological error model with unreliable measurements [7]; see Refs. [22,23]. More recently, attention has turned to tailoring the decoder to perform under more realistic types of noise, such as depolarizing noise [16–18,24,25] and correlated errors [26–28]. Of particular note is noise that is biased towards dephasing: a common feature of many architectures. With biased noise and reliable measurements, it is known that the surface code can be tailored to accentuate commonly occurring errors such that an appropriate decoder will give substantially increased thresholds [29,30]. However, these high thresholds were obtained using decoders with no known efficient implementation in the realistic setting where measurements are unreliable and the noise bias is finite.

In this Letter we propose a practical and efficient decoder that performs well for both finite bias and noisy measurements, demonstrating that the exceptional gains of the tailored surface code under biased noise extend to the fault-tolerant regime. We use the MWPM algorithm together with a recent technique to exploit symmetries of a given

quantum error-correcting code [31]. Rather than using the symmetries of the code, we generalize this idea and use the symmetries of the entire system. Specifically, we exploit the symmetries of the syndrome with respect to its incident error model. Applied to pure dephasing noise, our decoder exploits the one-dimensional symmetries of the system by pairing the defects of each symmetry separately. Crucially, our approach readily extends to the situation where measurements are unreliable, as well as the finite-bias regime where some low-rate errors violate the symmetries we rely on. We demonstrate that our approach leads to fault-tolerant thresholds exceeding 6% for infinite bias, with these substantial gains persisting to modest biases. Comparing with the *optimal* threshold of 3.3% [22,23] for conventional decoders that correct the bit-flip and dephasing errors of the same noise model separately, our results represent a very significant improvement in the level of noise that can be tolerated in practical quantum technologies.

Surface code tailored for dephasing.—We define the surface code in a rotated basis with X- and Y-type stabilizers, $S_v \in \mathcal{S}$, to provide additional syndrome information about Z errors; see Fig. 1 and its corresponding caption. We consider errors $E \in \mathcal{E}$ drawn from a subgroup of the Pauli group $\mathcal{E} \subseteq \mathcal{P}$. We define the syndrome as a list of the locations of defects. For a given error, defects lie on vertices v such that $S_v E|\psi\rangle = (-1)E|\psi\rangle$ for code states $|\psi\rangle$ satisfying $S_v|\psi\rangle = |\psi\rangle$ for all v.

Decoding with symmetry.—We first consider the infinite bias (pure-dephasing) error model generated by only Z errors, $\mathcal{E}^Z = \langle Z_f \rangle$. Errors drawn from this model respect one-dimensional symmetries of the lattice, as in Fig. 1. A single Z error generates two defects on each of its adjacent rows and columns. Up to boundary conditions, any error drawn from $\mathcal{E}^Z$ will respect a defect parity conservation symmetry on each of the rows and columns of the lattice.
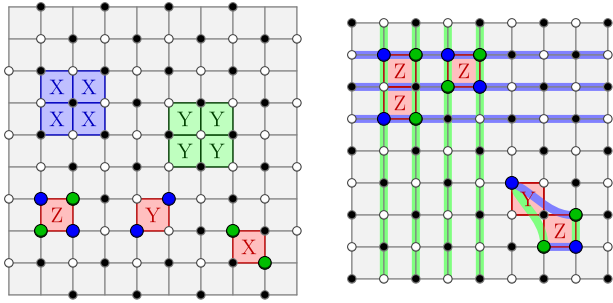
FIG. 1. (Left) The surface code with qubits on the faces of a square $d \times d$ lattice. The vertices v are bicolored such that stabilizer generators $S_v = \prod_{\partial f \ni v} X_f$ ($S_v = \prod_{\partial f \ni v} Y_f$) lie on black (white) vertices, and $\partial f \ni v$ denotes the faces f touching v. Examples are shown at the top of the figure. The syndrome patterns for Pauli X, Y, and Z errors are shown at the bottom of the figure. (Right) The surface code with periodic boundary conditions. Our noise model is such that Z errors occur at a higher rate than Pauli X or Y errors. The syndromes of Z errors, shown at the top left of the figure, respect one-dimensional symmetries, shown as blue and green lines. We can therefore consistently match vertices along the rows and columns of the lattice. The edges returned from each MWPM subroutine reproduce the boundary of the faces that support the error. Lower-rate non-dephasing errors may violate the symmetries of the system (bottom, right).

Let us make this notion of a symmetry rigorous. A symmetry is specified by a subgroup of the stabilizer group $\mathcal{S}_{\text{sym}} \subseteq \mathcal{S}$. Elements $S \in \mathcal{S}_{\text{sym}}$ are defined with respect to an error model $\mathcal{E}$ such that they satisfy $SE|\psi\rangle = (+1)E|\psi\rangle$ for all $E \in \mathcal{E}$ and code states $|\psi\rangle$. This generalizes Ref. [31] where symmetries are defined for the special case where $\mathcal{E} = \mathcal{P}$; the symmetry is now a function of the combined system of both the code and the error model.

For general Pauli error models, the surface code has global symmetries [2]; $\prod_{v \in \mathcal{G}} S_v = 1$ with $\mathcal{G}$ the set of either black or white vertices where we briefly assume periodic boundary conditions to illustrate this point. Under pure dephasing noise, the same model has a much richer set of one-dimensional symmetries. Observe that $S_{\mathcal{L}} = \prod_{v \in \mathcal{L}} S_v$, with $\mathcal{L}$ the set of vertices on a row or column, is a product of Pauli Z matrices. As such, the one-dimensional stabilizers $S_{\mathcal{L}}$ commute with errors drawn from $\mathcal{E}^Z$ and are therefore symmetries. The set of all such $S_{\mathcal{L}}$ generate $\mathcal{S}_{\text{sym}}$ with respect to $\mathcal{E}^Z$.

Now consider what this symmetry implies for an arbitrary syndrome in our error model. A direct consequence of the definition of a symmetry $\mathcal{S}_{\text{sym}}$ is that, for pure dephasing noise, there will always be an even number of defects measured by the subsets of stabilizers whose product gives elements of $\mathcal{S}_{\text{sym}}$. We can design a decoder that exploits this property of these subsets. Specifically, we can consistently pair the defects detected by the stabilizers of these subsets using, say, MWPM, or another suitable pairing algorithm such as that of Ref. [32]. Collections of

defects that are combined with pairing operations on sufficiently many symmetries can be neutralized with a low-weight Pauli operator. We say that such a collection is locally correctable [31]. For the surface code under pure dephasing noise, by performing pairing over the one-dimensional lattice symmetries, the edges returned from MWPM form the boundary of the error; see Fig. 1(right). The interior of the boundary determines the correction.

Such a decoder is readily extended to the fault-tolerant setting where measurements are unreliable and may give incorrect outcomes. A single measurement error will violate the defect symmetries of the two-dimensional system. Following the approach of Ref. [1], we can recover a new symmetry in the fault-tolerant setting in $(2 + 1)$-dimensional spacetime by repeating stabilizer measurements over time, see also Ref. [31]. A symmetry is recovered by taking the parity of pairs of sequential measurement outcomes, with odd parity heralding a defect. This spacetime symmetry is generic to our proposal here. In this situation, up to the lattice boundaries, the symmetries represent constraints among collections of defects lying on $(1 + 1)$-dimensional planes. Curiously, unlike the phenomenological bit-flip noise model for the surface code [7,33], the biased phenomenological error model considered here is anisotropic in spacetime. We emphasize the importance of checking for temporal logical errors, consisting of strings of sequential measurement errors, as they may introduce logical failures while performing code deformations [34].

The symmetries of the system are altered at lattice boundaries. We can adapt the decoder to account for this by adding a pair of defects at each time step to all vertices where a stabilizer is not imposed at the boundary; see Fig. 1 (left). These defects can be paired to other defects within their respective $(1 + 1)$-dimensional planes of symmetry. Otherwise, they can be matched together freely in the case that they do not need to be paired.

Decoding with finite bias.—We next adapt our decoder to deal with low-rate X and Y errors in addition to high-rate Z errors. For simplicity we will describe this modification for the case of periodic boundary conditions and where measurements are reliable. We give a technical description of all the decoders we present in the Supplemental Material [35].

The decoder for infinite bias noise will pair each defect of the system twice: once to a horizontally separated defect and once to a vertically separated defect. Low rate X and Y errors violate the one-dimensional symmetries that enable us to use the strategy described above, but we can weakly adhere to the strategy as follows. In our modified decoder we pair all defects twice: once where we strongly bias the decoder to pair defects horizontally, and a second time where we strongly bias each defect to pair vertically. Unlike in the infinite-bias case, we permit our decoder to pair defects that are not within their same row or column. We penalize such pairings according to the amount of noise

bias. This can be achieved in our input into the MWPM algorithm by assigning high weights to edges for pairs of defects that are not aligned on the same row or column, depending on the respective matching.

In the case of finite bias the collections of defects that are connected through the edges returned by pairing may not be locally correctable. We deal with this issue with additional use of MWPM to complete the decoding procedure. One can show that there will be an even number of defects in each collection of defects connected by edges. Therefore, the parity of defects on black and white vertices are equal. We call collections of defects with an even (odd) parity of defects on black and white vertices "neutral" ("charged"). Neutral clusters can be locally corrected. Remaining charged collections of defects can be made neutral by pairing them with other nearby charged collections of defects. This final pairing ensures the collections of connected defects are locally correctable.

Biased noise models.—We will test our decoder under two scenarios: with a biased noise model and ideal measurements, and with a phenomenological biased noise model with unreliable measurements. At each time step, qubits are subjected to an error with probability p. Pauli Z errors occur at high rate $p_{h.r.} = p\eta/(\eta + 1)$, while X and Y errors occur at a lower rate, $p_{l.r.} = p/2(\eta + 1)$. The phenomenological (ideal-measurement) biased noise model gives an incorrect measurement outcome with probability $q = p$ ($q = 0$).

It is important to consider whether the phenomenological noise model we introduced is compatible with a noise-bias setting [36]. As we now demonstrate, it is possible to measure stabilizers and maintain the bias. Following the standard approach [1], stabilizers are measured by preparing an ancilla a in an eigenstate of X, then applying entangling gates between the ancilla and the qubits that support the stabilizer, and finally measuring the ancilla qubit in the X basis. To measure S_v for black vertices v we apply $\prod_{\partial f \ni v} CX_{a,f}$, where $CX_{a,f} = (1 + Z_a + X_f - Z_a X_f)/2$ is the controlled-not gate. To measure white vertex stabilizers, we replace the $CX_{a,f}$ gates with $CY_{a,f}$ gates. These gates differ by an $\exp(i\pi Z_f/2)$ rotation.

We can now justify that stabilizer measurements performed this way preserve the noise bias. Specifically, we demonstrate that no steps in the stabilizer circuit cause high-rate errors to introduce X or Y errors to the data qubits of the surface code. The $CX_{a,f}$ commutes with Z errors that act on the ancilla. As such, it will not create high rate X or Y errors on the data qubits. Similarly, the single-qubit rotation that maps $CX_{a,f}$ onto $CY_{a,f}$ commutes with the high-rate errors, and will therefore only map low-rate errors onto other low-rate errors. Ancilla qubits are vulnerable to high-rate Pauli Z errors. This is reflected by the error model that has a high measurement error rate, $q = p$. An additional concern is that the entangling gates such as $CX_{a,f}$ may increase the frequency that low-rate errors occur. This will

depend on the physical implementation, and recent proposals have demonstrated that noise-bias-preserving $CX_{a,f}$ gates are indeed possible in some architectures [37].

Numerical simulations.—We simulate the performance of our decoder for the surface code with periodic boundary conditions against the phenomenological biased noise model, using 30 000 trials per code distance and physical error probability. We used the critical exponent method of Ref. [7], fitting to a quadratic model, to obtain threshold estimates with jackknife resampling over code distances to determine error bounds. Because of the anisotropy in spacetime, we might expect the thresholds of logical errors in the spatial and temporal direction to differ. We report a failure if a logical error occurs in either the spatial or temporal direction. Our results are shown in Fig. 2. We identify a threshold of 6.32(3)% for pure dephasing, and thresholds of ∼5% for biases around $\eta = 100$. Our decoder begins to outperform the optimal values for standard methods, where bit-flip and dephasing errors are corrected separately, at $\eta \sim 5$. These results demonstrate the advantage of using our decoder in the fault-tolerant setting, even if the noise bias is modest.

We have simulated the performance on the surface code with boundaries, yielding similar results. Figure 3 demonstrates a threshold using the fault-tolerant decoder for the surface code with boundaries where $\eta = 100$. In this case we only measure spatial logical errors because there are no topologically nontrivial temporal errors. Remarkably, the
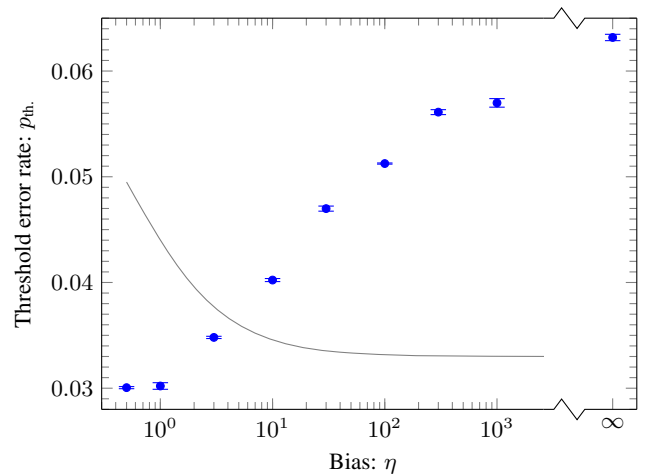

FIG. 2. Threshold error rates p_{th} as a function of noise bias η for both spatial and temporal logical errors for the surface code with periodic boundary conditions. The points show threshold estimates together with 1 standard deviation error bars. The points at smallest and largest bias values correspond to $\eta = 0.5$ (depolarizing noise), and $\eta = \infty$ (pure dephasing), respectively. The solid line represents the optimal performance for the standard surface code with phenomenological noise of a decoder that deals with bit-flip errors and dephasing noise separately. Codes with distance $d = 12, 14, 16, 18, 20$ and $d = 24, 28, 32, 36, 40$ were used for finite and infinite bias threshold estimates, respectively.
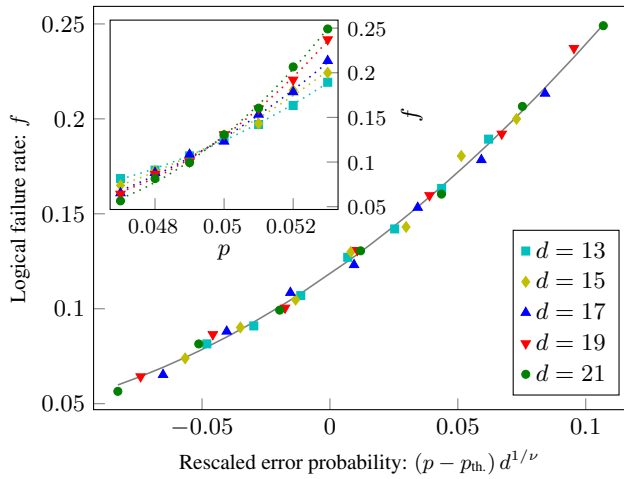
FIG. 3. Numerical data demonstrating a finite threshold in the fault-tolerant setting. Logical (spatial) failure rate f for the surface code with boundaries shown as a function of the rescaled error rate $x = (p - p_{th})d^{1/\nu}$ with bias $\eta = 100$ and $p_{th} = 4.96(1)\%$. The solid line is the best fit to the model $f = A + Bx + Cx^2$. The insets show the raw sample means over 30 000 runs for various values of p.

FIG. 4. Threshold error rates p_{th} as a function of noise bias η for the surface code with periodic boundary conditions and ideal measurements. The points show threshold estimates with 1 standard deviation error bars. The points at smallest and largest bias values correspond to $\eta = 0.5$ (depolarizing noise), and $\eta = \infty$ (pure dephasing), respectively. The solid line, which is the zero-rate hashing bound for the associated Pauli error channel, represents threshold error rates that are achievable with ML decoding [30]. Codes with distance $d = 24, 28, 32, 36, 40$ and $d = 48, 56, 64, 72, 80$ were used for finite and infinite bias threshold estimates, respectively.

threshold is very similar to the threshold obtained in the case with periodic boundary conditions where we also count logical failures along the temporal direction as well. This is surprising given the anisotropy of the decoding problem in the spatial and temporal directions.

We benchmark our decoder against the optimal performance of the surface code under the biased noise model. In the absence of optimal fault-tolerant thresholds (say, from statistical mechanical arguments [38]), we benchmark using the ideal measurement model. In this case, optimal performance corresponds to the zero-rate hashing bound, which is achievable using a ML decoder [16,30]. We see in Fig. 4 that our decoder underperforms in comparison to the ML decoder, suggesting that there is considerable scope for further improvements. A natural proposal would be to incorporate belief propagation into the MWPM algorithm. Choices of boundary conditions also play a role. We note that our decoder applied to the surface code with boundaries can achieve the optimal threshold of $p_{th} \sim 1/2$ for pure dephasing noise. However, it underperforms similarly to that shown in Fig. 4 at finite biases.

Low error rates.—The performance of the decoder below threshold will determine the resources required to perform quantum computation. We now speculate on the logical failure rates where the physical error rate is low, specifically $p \ll 1/d$. Using conventional decoding methods the logical failure rate decays as $\mathcal{O}(p^{\delta\sqrt{n}})$ [1,39] with $n = d \times d$ the code length and δ a constant. The high-threshold at infinite bias is indicative that the decoder can tolerate up to $\sim n/2$ dephasing errors [29,30]. We may therefore expect that the logical failure rate will decay with improved scaling, $\mathcal{O}(p_{h.r.}^{\alpha n})$, for some constant α.
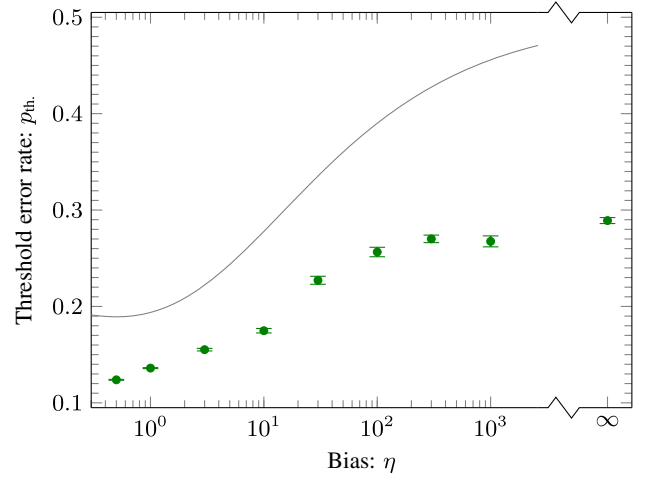
At finite noise bias, the improved scaling in logical failure rate with n can only persist up to some critical system size. Above some system size that depends on η, we expect that the most likely error that will cause a logical failure will be due a string consisting of $\sim\sqrt{n}$ low-rate errors. Up to constant factors, this will occur for some n where $p_{h.r.}{}^{\alpha n} \ll p_{l.r.}{}^{\delta\sqrt{n}}$. Nevertheless, given high bias, the decoder will vastly improve logical error rates in the regime where the most likely failure mechanisms are due to long strings of low-rate error events.

We contrast this with bias nullification schemes by concatenation [40,41]. These approaches increase the effective rate that uncommon errors act on the surface code by a factor equal to the number of qubits of each repetition code, leading to worse performance at low error rates. Moreover, they can only tolerate at most $\propto \sqrt{n}$ high-rate errors.

Extending again to the fault-tolerant case, temporal-logical errors are caused by strings of measurement errors that occur at a high rate. We should consider increasing the number of repetitions T of the error-correction cycle between code deformations to reduce the likelihood of temporal logical failures. Choosing $T \sim 2\delta\sqrt{n}\log p_{l.r.}/\log p$ will ensure temporal errors will occur at a rate similar to spatial logical errors, $\sim p_{l.r.}{}^{\delta\sqrt{n}}$, where we have assumed a temporal logical error occurs with likelihood $\sim p^{T/2}$. To achieve the target logical failure rate of the system, although the qubits will be occupied for a longer time to

decrease the failure rate of temporal logical errors, the associated decrease in the two spatial dimensions will result in a net improvement on resource scaling using our system.

Discussion.—Minimum-weight perfect matching has formed the backbone of topological quantum error correction [1,7,19,31,33,42,43]. The realization that we can design MWPM decoders with knowledge of the symmetries of the code or system opens up a number of new avenues for decoding algorithm design. A multitude of codes have yet to be explored, as well as their interaction with specialized noise models that reflect the errors that occur in the laboratory. Significant improvements in fault-tolerant thresholds obtained though tailored codes and realistic noise models, such as those we have demonstrated here, offer great promise for the realization of practical quantum technologies.

[1] E. Dennis, A. Kitaev, A. Landahl, and J. Preskill, Topological quantum memory, J. Math. Phys. (N.Y.) **43,** 4452 (2002).

[2] A. Yu. Kitaev, Fault-tolerant quantum computation by anyons, Ann. Phys. (Amsterdam) **303,** 2 (2003).

[3] B. J. Brown, D. Loss, J. K. Pachos, C. N. Self, and J. R. Wootton, Quantum memories at finite temperature, Rev. Mod. Phys. **88,** 045005 (2016).

[4] E. T. Campbell, B. M. Terhal, and C. Vuillot, Roads towards fault-tolerant universal quantum computation, Nature (London) **549,** 172 (2017).

[5] B. M. Terhal, Quantum error correction for quantum memories, Rev. Mod. Phys. **87,** 307 (2015).

[6] R. Raussendorf and J. Harrington, Fault-Tolerant Quantum Computation with High Threshold in Two Dimensions, Phys. Rev. Lett. **98,** 190504 (2007).

[7] C. Wang, J. Harrington, and J. Preskill, Confinement-Higgs transition in a disordered gauge theory and the accuracy threshold for quantum memory, Ann. Phys. (Amsterdam) **303,** 31 (2003).

[8] S. Bravyi and A. Kitaev, Universal quantum computation with ideal Clifford gates and noisy ancillas, Phys. Rev. A **71,** 022316 (2005).

[9] B. J. Brown, A fault-tolerant non-Clifford gate for the surface code in two dimensions, arXiv:1903.11634.

[10] B. J. Brown, K. Laubscher, M. S. Kesselring, and J. R. Wootton, Poking Holes and Cutting Corners to Achieve Clifford Gates with the Surface Code, Phys. Rev. X **7,** 021029 (2017).

[11] C. Horsman, A. G. Fowler, S. Devitt, and R. Van Meter, Surface code quantum computing by lattice surgery, New J. Phys. **14,** 123011 (2012).

[12] R. Barends *et al.*, Superconducting quantum circuits at the surface code threshold for fault tolerance, Nature (London) **508,** 500 (2014).

[13] A. D. Córcoles, E. Magesan, S. J. Srinivasan, A. W. Cross, M. Steffen, J. M. Gambetta, and J. M. Chow, Demonstration of a quantum error detection code using a square lattice of four superconducting qubits, Nat. Commun. **6,** 6979 (2015).

[14] J. Kelly *et al.*, State preservation by repetitive error detection in a superconducting quantum circuit, Nature (London) **519,** 66 (2015).

[15] M. Takita, A. D. Córcoles, E. Magesan, B. Abdo, M. Brink, A. W. Cross, J. M. Chow, and J. M. Gambetta, Demonstration of Weight-Four Parity Measurements in the Surface Code Architecture, Phys. Rev. Lett. **117,** 210505 (2016).

[16] S. Bravyi, M. Suchara, and A. Vargo, Efficient algorithms for maximum likelihood decoding in the surface code, Phys. Rev. A **90,** 032326 (2014).

[17] A. S. Darmawan and D. Poulin, Linear-time general decoding algorithm for the surface code, Phys. Rev. E **97,** 051302 (2018).

[18] G. Duclos-Cianci and D. Poulin, Fast Decoders for Topological Quantum Codes, Phys. Rev. Lett. **104,** 050504 (2010).

[19] A. G. Fowler, M. Mariantoni, J. M. Martinis, and A. N. Cleland, Surface codes: Towards practical large-scale quantum computation, Phys. Rev. A **86,** 032324 (2012).

[20] J. Edmonds, Paths, trees and flowers, Can. J. Math. **17,** 449 (1965).

[21] V. Kolmogorov, Blossom V: A new implementation of a minimum cost perfect matching algorithm, Math. Program. Comput. **1,** 43 (2009).

[22] A. Kubica, M. E. Beverland, F. Brandão, J. Preskill, and K. M. Svore, Three-Dimensional Color Code Thresholds Via Statistical-Mechanical Mapping, Phys. Rev. Lett. **120,** 180501 (2018).

[23] T. Ohno, G. Arakawa, I. Ichinose, and T. Matsui, Phase structure of the random-plaquette Z_2 gauge model: Accuracy threshold for a toric quantum memory, Nucl. Phys. **B697,** 462 (2004).

[24] A. G. Fowler, Optimal complexity correction of correlated errors in the surface code, arXiv:1310.0863.

[25] J. R. Wootton and D. Loss, High Threshold Error Correction for the Surface Code, Phys. Rev. Lett. **109,** 160503 (2012).

[26] A. G. Fowler, A. C. Whiteside, A. L. McInnes, and A. Rabbani, Topological Code Autotune, Phys. Rev. X **2,** 041003 (2012).

[27] A. Hutter and D. Loss, Breakdown of surface-code error correction due to coupling to a bosonic bath, Phys. Rev. A **89,** 042334 (2014).

[28] N. H. Nickerson and B. J. Brown, Analysing correlated noise in the surface code using adaptive decoding algorithms, Quantum **3,** 131 (2019).

[29] D. K. Tuckett, S. D. Bartlett, and S. T. Flammia, Ultrahigh Error Threshold for Surface Codes with Biased Noise, Phys. Rev. Lett. **120,** 050505 (2018).

[30] D. K. Tuckett, C. T. Chubb, S. Bravyi, S. D. Bartlett, and Steven T. Flammia, Tailoring Surface Codes for Highly Biased Noise, Phys. Rev. X **9**, 041031 (2019).

[31] B. J. Brown and D. J. Williamson, Parallelized quantum error correction with fracton topological codes, Phys. Rev. Research **2**, 013303, (2020).

[32] N. Delfosse and N. H. Nickerson, Almost-linear time decoding algorithm for topological codes, arXiv:1709 .06218.

[33] R. Raussendorf, J. Harrington, and K. Goyal, A fault-tolerant one-way quantum computer, Ann. Phys. (Amsterdam) **321**, 2242 (2006).

[34] C. Vuillot, L. Lao, B. Criger, C. G. Almudéver, K. Bertels, and B. M. Terhal, Code deformation and lattice surgery are gauge fixing, New J. Phys. **21**, 033028 (2019).

[35] See Supplemental Material at http://link.aps.org/ supplemental/10.1103/PhysRevLett.124.130501 for a technical description of the decoders implemented in the paper.

[36] P. Aliferis and J. Preskill, Fault-tolerant quantum computation against biased noise, Phys. Rev. A **78**, 052331 (2008).

[37] S. Puri, L. St-Jean, J. A. Gross, A. Grimm, N. E. Frattini, P. S. Iyer, A. Krishna, S. Touzard, L. Jiang, A. Blais, S. T. Flammia, and S. M. Girvin, Bias-preserving gates with stabilized cat qubits, arXiv:1905.00450.

[38] C. T. Chubb and S. T. Flammia, Statistical mechanical models for quantum codes with correlated noise, arXiv: 1809.10704.

[39] M. E. Beverland, B. J. Brown, M. J. Kastoryano, and Q. Marolleau, The role of entropy in topological quantum error correction, J. Stat. Mech. (2019) 073404.

[40] A. M. Stephens, W. J. Munro, and K. Nemoto, High-threshold topological quantum error correction against biased noise, Phys. Rev. A **88**, 060301(R) (2013).

[41] X. Xu, Q. Ahao, X. Yuan, and S. C. Benjamin, High-Threshold Code for Modular Hardware With Asymmetric Noise, Phys. Rev. Applied **12**, 064006 (2019).

[42] N. Delfosse, Decoding color codes by projection onto surface codes, Phys. Rev. A **89**, 012317 (2014)

[43] A. Kubica and N. Delfosse, Efficient color code decoders in $d \geq 2$ dimensions from toric code decoders, arXiv: 1905.07393.